Paleoceanography and Paleoclimatology

RESEARCH ARTICLE
10.1029/2018PA003470

Mitigation of Extreme Ocean Anoxic Event Conditions by Organic Matter Sulfurization

D. Hülse[1,2], S. Arndt[2,3], and A. Ridgwell[1,2]

[1]Department of Earth Sciences, University of California, Riverside, CA, USA, [2]BRIDGE, School of Geographical Sciences, University of Bristol, Bristol, UK, [3]BGeosys, Department Geoscience, Environment and Society (DGES), Université Libre de Bruxelles, Brussels, Belgium

Key Points:
- The impact of organic matter sulfurization on C and O_2 cycling during Ocean Anoxic Events is quantified by means of 3-D Earth system modeling
- Organic matter sulfurization reduces the extent and intensity of toxic euxinic conditions as well as H_2S emissions to the atmosphere
- Organic matter sulfurization drives enhanced OM burial, draws down atmospheric CO_2, and accelerates climate cooling and OAE recovery

Supporting Information:
- Supporting Information S1
- Figure S1

Correspondence to:
D. Hülse,
dominik.huelse@ucr.edu

Citation:
Hülse, D., Arndt, S., & Ridgwell, A. (2019). Mitigation of extreme ocean anoxic event conditions by organic matter sulfurization. *Paleoceanography and Paleoclimatology*, *34*, 476–489. https://doi.org/10.1029/2018PA003470

Received 30 AUG 2018
Accepted 4 MAR 2019
Accepted article online 15 MAR 2019
Published online 5 APR 2019

Abstract Past occurrences of widespread and severe anoxia in the ocean have frequently been associated with abundant geological evidence for free hydrogen sulfide (H_2S) in the water column, so-called euxinic conditions. Free H_2S may react with, and modify, the chemical structure of organic matter settling through the water column and in marine sediments, with hypothesized implications for carbon sequestration. Here, taking the example of Ocean Anoxic Event 2, we explore the potential impact of organic matter sulfurization on marine carbon and oxygen cycling by means of Earth system modeling. Our model experiments demonstrate that rapid sulfurization ($k_{sulf} \geq = 10^5$ M^{-1} $year^{-1}$) of organic matter in the water column can drive a more than 30% enhancement of organic carbon preservation and burial in marine sediments and hence help accelerate climate cooling and Ocean Anoxic Event 2 recovery. As a consequence of organic matter sulfurization, we also find that H_2S can be rapidly scavenged and the euxinic ocean volume reduced by up to 80%—helping reoxygenate the ocean as well as reducing toxic H_2S emissions to the atmosphere, with potential implications for the kill mechanism at the end-Permian. Finally, we find that the addition of organic matter sulfurization induces a series of additional feedbacks, including further atmospheric CO_2 drawdown and ocean reoxygenation by the creation of a previously unrecognized net source of alkalinity to the ocean as H_2S is scavenged and buried.

1. Introduction

Oceanic Anoxic Events (OAEs) are severe perturbations of global biogeochemical cycling associated with widespread deposition of laminated organic matter-rich sediments under anoxic/euxinic conditions—so-called black shales (Schlanger & Jenkyns, 1976). Originally envisaged as encompassing a series of three major and five minor events that occurred during the Jurassic and Cretaceous periods (Jenkyns, 2010), evidence for the transient occurrence of extensive ocean anoxia/euxinia has also been found associated with the Late Ordovician, Late Devonian, end-Permian, and Early Jurassic extinction events (Meyer & Kump, 2008). Hydrogen sulfide (H_2S) in the water column is produced from bacterial sulfate reduction once more powerful terminal electron acceptors, like oxygen, are depleted. Thought to be important to the occurrence of euxinic conditions are a warm climate and a nutrient-trapping geography, such as in restricted basins that were predisposed to euxinia (Meyer & Kump, 2008). Many OAEs are also linked to episodes of enhanced volcanism and the emplacement of flood basalts, providing a mechanism to drive climate warming (via elevated atmospheric CO_2 concentrations; Naafs et al., 2016) and ocean deoxygenation, via reduced O_2 solubility and increased phosphate weathering and hence ocean productivity (Flögel et al., 2011; Monteiro et al., 2012; Wallmann, 2001). Plausible OAE triggering mechanisms are hence known, even if not necessarily explored yet in any great mechanistic and dynamical detail. This leaves the primary outstanding question: What is (are) the dominant mechanism(s) by which the Earth system recovers from such extreme conditions?

There are two main purported mechanisms to drown atmospheric CO_2 and cool and reoxygenate the oceans: (1) enhanced organic carbon burial in marine sediments and (2) enhanced silicate mineral weathering on the continents with subsequent carbonate burial in marine sediments (e.g., Berner, 1999; Ridgwell & Zeebe, 2005). However, geochemical evidence from OAE2, for example, suggests that the climate recovery was faster than can be explained by enhanced silicate and carbonate weathering alone (Kuypers et al., 1999; Pogge von Strandmann et al., 2013; Wallmann, 2001) and, thus, emphasizes the important role of OM

burial in terminating anoxic events (Arthur et al., 1988). Enhanced burial of OM removes CO_2 from the ocean/atmosphere system and thus induces global cooling. At the same time the accumulation of O_2 in the atmosphere and surface waters has been shown to act as a negative feedback, eventually leading to the reoxygenation of the deeper ocean and a subsequent shutdown of the positive feedback between anoxia, enhanced P recycling and increased productivity (Handoh & Lenton, 2003; Tsandev & Slomp, 2009; Van Cappellen & Ingall, 1994). While not a true OAE per se, recovery from the warming transient at the Paleocene-Eocene boundary ("PETM") is also inferred to have been amplified by enhanced organic matter burial and not just driven by silicate weathering alone (Bowen & Zachos, 2010; Gutjahr et al., 2017). If so, the greatest outstanding unknown shifts to the specific means by which organic carbon burial is enhanced during OAEs.

Long-established explanations for increased OM burial during OAEs infer increased productivity and/or an increased preservation of OM (Demaison & Moore, 1980; Pedersen & Calvert, 1990). Their relative importance is most likely dynamic, but difficult to assess. Elevated marine productivity and carbon export from the ocean surface very likely played an important role for triggering and maintaining OAEs, potentially driven by an increased source of phosphate from continental weathering in conjunction with reduced removal due to efficient phosphate regeneration under anoxic conditions (Van Cappellen & Ingall, 1994). Indeed, previous Earth system modeling has been unable to explain the observed widespread occurrence of anoxic and euxinic conditions without invoking at least a doubling of ocean phosphate inventory and hence marine productivity (Monteiro et al., 2012; Ruvalcaba Baroni et al., 2014; Tsandev & Slomp, 2009). Yet, unlike preservation, increased productivity is not an efficient recovery mechanism as only a very small fraction of the carbon fixed in OM is sequestered in the sediments for longer time scales (Volk & Hoffert, 1985). The majority of OM is remineralized in the upper ocean, releasing CO_2 and intensifying ocean anoxia due to increased oxidant demand. In contrast, enhanced OM preservation increases the removal of fixed carbon from the ocean/atmosphere system as well as the net oxygen gain by the ocean and atmosphere. Enhanced OM preservation could thus have been critical to the recovery from OAEs. Previously, enhanced OM preservation during OAEs has been explained by reduced degradation rates under anoxic environmental conditions (e.g., Demaison & Moore, 1980; LaRowe & Van Cappellen, 2011), potentially supplemented by physical protection of OM as a consequence of higher clay mineral availability (Kennedy et al., 2002). A further but less widely recognized factor involves the reaction of labile OM compounds, such as functionalized lipids and carbohydrates, with reduced inorganic sulfur species (e.g., H_2S), resulting in sulfur cross-linked macromolecular networks (Sinninghe Damsté et al., 1988) that are more resistant to bacterial degradation and thus exhibit an enhanced preservation potential (Sinninghe Damsté et al., 1998).

Intense sulfurization of black shale OM has been previously described for sediments from Tarfaya Basin (e.g., Kolonic et al., 2002, 2005), Demerara Rise (e.g., Böttcher et al., 2006; Hetzel et al., 2009), Pont d'Issole (Raven et al., 2018), or the Jurassic Kimmeridge Clay Formation (e.g., Sinninghe Damsté et al., 1998; van Kaam-Peters et al., 1997, 1998; van Dongen et al., 2006). At all these sites, intense OM sulfurization is linked to enhanced OM burial. For instance, based on a comprehensive geochemical analysis of samples from the Kimmeridge Clay Formation, van Kaam-Peters et al. (1997, 1998) and van Dongen et al. (2006) showed that OM contents can be quantitatively linked to the degree of OM sulfurization. Kolonic et al. (2005) estimated that OAE2 mass accumulation rates at Tarfaya Basin would result in unrealistically high export production if one assumed a purely productivity controlled OM burial flux. They thus conclude that the enhanced preservation of sulfurized OM increased OM burial at the Tarfaya Basin site. Furthermore, using an inverse reaction-transport model approach, Arndt et al. (2006, 2009) demonstrated that intensely sulfurized OM, found in black shale sequences at Demerara Rise, is characterized by extremely low OM degradability and, thus, high preservation efficiencies of more than 80% (sometimes close to 100%) of total deposited black shale OM. These model estimates corroborate the findings of earlier lab experiments with sulfurized sapropel OM revealing that this substrate is quasi unavailable for sulfate reducers, resulting in a close to 100% preservation (Moodley et al., 2005).

Despite observational evidence advocating the importance of OM sulfurization for local OM burial during OAEs, its impact on global biogeochemical cycling and climate and, thus, its significance for Earth system recovery from OAEs is essentially unconstrained. Early observations suggested that OM is sulfurized during early diagenesis over time scales ranging from decades to several thousand years (e.g., Wakeham et al., 1995; Werne et al., 2000). Although such slow OM sulfurization can support an enhanced OM preservation during burial in marine sediments, it cannot serve as an efficient recovery mechanism that rapidly sequesters OM, reduces atmospheric CO_2, and alleviates water column anoxia/euxinia. However, labora-

tory experiments provide evidence for more rapid OM sulfurization (on the order of weeks, e.g., Adam et al., 1998; Kok et al., 2000; van Dongen et al., 2003). In addition, more recent studies in the Cariaco Basin show that reduced sulfur can be rapidly incorporated into sinking OM within days or less (Li et al., 2011; Raven et al., 2016). Small changes in redox stratification, for instance, driven by changes in export production or ocean circulation could thus trigger large changes in sulfurization and OM sequestration (Raven et al., 2018). As a consequence, rapid water column OM sulfurization could be an initially very efficient mechanism for drawing down CO_2 and H_2S and thus inducing the Earth system's recovery from OAEs. However, although sulfurization of OM is considered by some authors a globally significant process for preserving organic compounds (Arndt et al., 2009; Raven et al., 2018; Sinninghe Damsté et al., 1998), the dynamic interplay between primary productivity, ocean redox conditions, OM sulfurization, and its preservation in the sediments has yet to be examined.

In this paper, we quantitatively explore the role of OM sulfurization as a global recovery mechanism from ocean anoxic events. More specifically, we test if the occurrence of euxinic conditions and the rates of OM sulfurization in the water column can be sufficient to create an appreciable enhancement of OM sequestration in marine sediments. We use an Earth system model to quantify the impact of this process on key ocean biogeochemical cycles and take as an example event, the archetypal Cenomanian-Turonian boundary OAE (OAE2, ~93.5 Ma), characterized by high global temperatures caused by elevated atmospheric CO_2 (Friedrich et al., 2012), enhanced primary productivity (Schlanger & Jenkyns, 1976), widespread anoxia (e.g., Brumsack, 2006; Goldberg et al., 2016; Owens et al., 2012), and euxinia with free H_2S in the water column (Monteiro et al., 2012; Pancost et al., 2004; Sinninghe Damsté & Köster, 1998).

2. Methods

For our numerical model experiments, we employ the cGENIE model, which is based on a 3-D-ocean circulation and a 2-D energy-moisture balance atmosphere model (Edwards & Marsh, 2005) and coupled to marine biogeochemical cycling of carbon, oxygen, phosphorus, and sulfur (Monteiro et al., 2012; Ridgwell et al., 2007). Here, cGENIE is implemented on a 36 × 36 equal-area horizontal grid with 16 vertical levels in the ocean and uses Cenomanian bathymetry and continental configuration identical to Monteiro et al. (2012) and Zhou et al. (2015, and see supporting information). Monteiro et al. (2012) evaluated the cGENIE setup for the Late Cretaceous and assessed the role of paleogeography, atmospheric CO_2, and oceanic nutrient content on the distribution of ocean redox conditions. They showed that ocean phosphate content is the main lever for the model to successfully simulate observed patterns of ocean anoxia/euxinia for before and during OAE2. Further model evaluation is provided in Zhou et al. (2015), showing that simulated regional differences in oxygen levels in the proto-North Atlantic Ocean are consistent with the paleoredox proxy I/Ca. We implement a couple of changes compared to the configuration of Monteiro et al. (2012). First, we add a representation of OM sulfurization in the water column. In this, the more labile pool of sinking OM represented in cGENIE (see Ridgwell et al., 2007) is subject to sulfurization in the presence of free H_2S, which we implement via a bimolecular rate law controlled by rate constant k_{sulf} (see supporting information). Sinking sulfurized OM is hence transferred to the refractory pool and is not subject to further alteration or degradation in the water column and sediments. Note that this is an end-member scenario in that we do not consider here the possibility of partial remineralization of sulfurized OM occurring. However, our assumption is but supported by observations and model results (Arndt et al., 2006, 2009; Moodley et al., 2005). Second, to simplify the analysis of sulfurization impacts, we omit nitrogen dynamics (and hence consider PO_4 as the only nutrient, as per Meyer et al., 2016). This slightly shifts patterns of the highest primary productivity, however our model still successfully reproduces observed patterns of ocean redox conditions at the seafloor and in the photic zone (see supporting information). Furthermore, we couple the ocean biogeochemistry model to the new 1-D vertically resolved and fully coupled reaction-transport sediment model, "OMEN-SED" (Hülse et al., 2018). Therefore, giving us the ability to avoid having to impose reflective boundary conditions for organic carbon and hence artificially amplifying oxygen consumption at the seafloor (Hülse et al., 2017).

OMEN-SED describes the degradation and burial of two OM pools in the sediments, as well as associated biogeochemical dynamics of the most important terminal electron acceptors (here O_2, SO_4^{2-}) and methane (CH_4), and related reduced substances (H_2S). For this study, we omit phosphorus dynamics in OMEN-SED and its regeneration under anoxic conditions. Instead, in our initial steady-state experiments, all organic phosphorus raining down on the seafloor gets instantaneously recycled and returned to the deepest ocean grid-cell as phosphate (PO_4), thus fixing the global PO_4 inventory. (We will address the role of longer-term

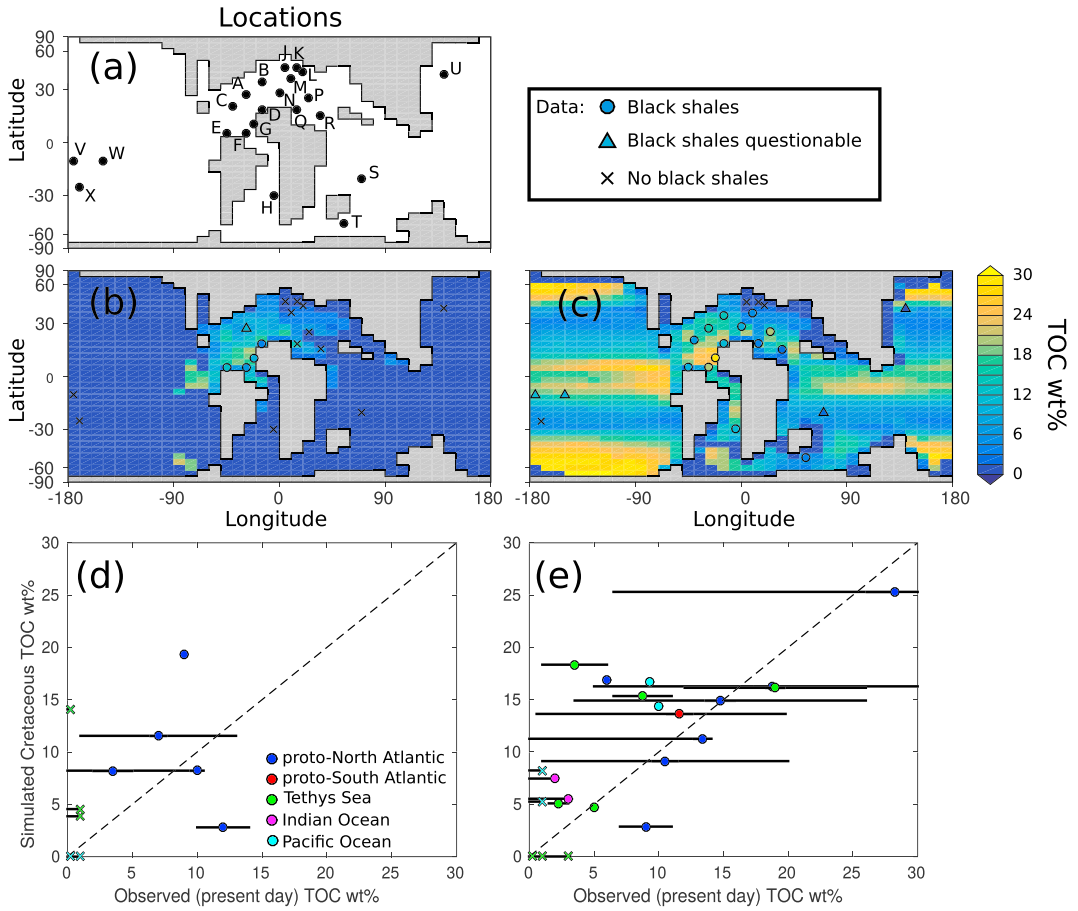

Figure 1. Global distribution of TOC wt% as reported in Table 1. Locations of observations (a), simulated TOC wt% at 1-m sediment depth for a pre-OAE2 simulation with $1 \times [PO_4]$ (b) and peak-OAE2 with $2 \times [PO_4]$ (c), both with observations superimposed and excluding OM sulfurization. Crossplots comparing simulated and observed TOC contents ((d) pre-OAE2; (e) peak-OAE2), with error bars indicating ranges of observed values reported for the specific location. TOC = total organic carbon.

feedbacks, e.g., involving PO_4 in a separate and subsequent paper.) Sediments also receive a nonbiogenic, noncarbonate detrital flux of 0.18 g·cm^{-2}·k.y.$^{-1}$, a value characteristic of early Cenozoic open-ocean sediments (Zeebe & Zachos, 2007). In OMEN-SED, the degradation rate constant for labile OM follows the tuned spatially uniform value of Hülse et al., 2018 (2018; $k_1 = 0.0065$ year^{-1}). We set the degradation rate constant for the refractory OM pool as a function of the oxygen concentration ($[O_2]$) of the overlying ocean waters (LaRowe & Van Cappellen, 2011)—k_2 taking a value of 0.001 year^{-1} for [O2] $\geq$ 5.0 μM, and $k_2 = 10^{-5}$ for [O2] < 5.0 μM (a value more representative for OM reactivity in Cretaceous black shales, Arndt et al., 2009). The entire sulfurized OM pool (together with the associated, scavenged H_2S) is assumed to be completely preserved in the sediments.

In our initial assessment of the impact of OM sulfurization on marine biogeochemical cycling, we explore the sensitivity of the system to two main controlling parameters (sulfurization rate and ocean nutrient inventory) and create an ensemble of model experiments. These experiments are carried out with atmospheric xCO_2 fixed at 4.0× preindustrial values (1,112 ppmv, as determined by Monteiro et al., 2012) and atmospheric xO_2 at modern (21,000 ppm). We set no weathering flux and hence deliberately do not attempt to account for the role of longer-term (ca. 10–100 kyr) feedbacks between OM burial, CO_2, ocean temperature, and oxygenation in these particular simulations. While organic carbon is preserved and buried in the sediments, we force a closure of the carbon cycle by means of the fixed atmospheric xCO_2 boundary condition (and hence preventing any climate feedback). All PO_4 in OM reaching the sediments, whether sulfurized or not, is returned to the ocean. While we allow the removal of OM associated H_2S, this loss is small compared to the initial ocean sulfate inventory of 29,160 μmol/kg (e.g., the total ocean dissolved sulfur changes

Table 1
Observations and Simulated TOC wt% During OAE2 (Pre-OAE2 Simulation With 1 × [PO_4] and Peak-OAE2 With 2 × [PO_4], Also Compare Figure 1)

		Black shales Observed		Total organic carbon wt% Observed		Simulated $k_{sulf} = 0$		Simulated $k_{sulf} = 10^5$	
Label	Locations	Pre	Peak	Pre	Peak	Pre	Peak	Pre	Peak
A	Cape Hatteras (DSDP sites 105, 603B)	✓	✓	<10	3.5–26	8.2	14.9	11.4	23.4
B	Newfoundland Basin (ODP Site 1276)	–	✓	–	13.4	7.5	11.3	9.2	16.3
C	Hatteras Abyss (ODP Site 1276)	–	✓	–	6	9.8	16.9	13.3	25.5
D	Tarfaya Basin (Morocco)	✓	✓	2–5	1–20	8.2	9.1	9.7	13.6
E	Maracaibo Basin (Venezuela)	✓	✓	10–14	7–11	2.8	2.9	2.9	3.2
F	Demerara Rise (DSDP site 144, ODP Leg 207)	✓	✓	1–13	5–32.5	11.5	16.3	14.5	24.0
G	Cape Verde (DSDP sites 367, 368)	✓	✓	9	6.5–50	19.3	25.3	22.9	31.8
H	Angola Basin (DSDP site 530A)	×	✓	low TOC	0.6–19.8	0.0	13.6	0.0	15.5
J	Eastbourne and Dover (UK)	×	×	<0.25	<0.25	0.0	0.0	0.0	0.0
K	Münsterland Basin (Germany)	×	×	<1	<3	0.0	0.0	0.0	0.0
L	Chrummflueschluch (Switzerland)	×	×	low TOC	low TOC	0.0	0.0	0.0	0.0
M	Vocontian Basin (France)	×	✓	<1	5	3.9	4.7	4.4	6.4
N	Galicia Margin (ODP Site 641)	–	✓	–	6.5–11	10.6	15.3	14.6	24.1
P	Apennines (Italy)	×	✓	–	12–26	0.0	16.1	3.5	24.7
Q	Oued Bahloul (Tunisia)	×	✓	–	1–6	14.1	18.3	17.4	25.8
R	Levant Platform (Jordan)	×	✓	< 1	1.5–3	4.5	5.1	5.0	6.7
S	Tethyan Himalayas (Tibet)	×	✓	–	<2	0.0	7.5	0.0	10.6
T	Kerguelen Plateau (ODP site 1138)	–	✓	–	<3	0.0	5.5	0.0	5.6
U	Yezo Group (Japan)	×	×	–	<1	0.0	8.2	0.0	8.2
V	Mariana Basin (DSDP site 585)	×	✓	–	10	0.0	14.4	0.0	17.9
W	Shatsky and Hess Rise (DSDP sites 305, 310)	–	✓	–	9.3	0.0	16.7	0.1	20.6
X	Central South Pacific (DSDP site 463)	×	×	<1	<1	0.0	5.2	0.0	7.4

Note. For locations reporting a range of TOC wt% the mean value is used for the model-data comparison, for locations with maximum or minimum TOC wt% this value is used and if evidence reports "low TOC" a value of 0.25 TOC wt% is used (as this is the minimum value reported in the database). A dash (–) indicates no observation for this site in the database. Observations adapted from Monteiro et al. (2012). For references and explanation of the evidence see Monteiro et al. (2012). TOC = total organic carbon; OAE2 = Ocean Anoxic Event 2.

less than 0.05% over the course of the experiment applying a moderate sulfurization rate constant of $k_{sulf} = 10^5$ M^{-1} $year^{-1}$). (We explore and discuss the role of feedbacks in an open system configuration subsequently.) We test a range of potential pre-OAE2 through peak-OAE2 nutrient inventories, by considering PO_4 inventories varying between ×1 and ×2 modern (in increments ×0.2 modern), following Monteiro et al. (2012). Simultaneously, for each of the different [PO_4] assumptions, we vary the OM sulfurization rate constant over a plausible range from $k_{sulf} = 10^3$ M^{-1} $year^{-1}$, reflecting slow diagenetic sulfurization (Sinninghe Damsté et al., 2007) to $k_{sulf} = 10^7$ M^{-1} $year^{-1}$ representing reaction kinetics similar to those of fast secondary redox reactions (e.g., H_2S reoxidation by O_2). We hence generate a 6 × 5 grid of experiments (30 in total) of differing [PO_4] versus k_{sulf} with each experiment run for 20,000 years to achieve steady-state.

3. Results

3.1. Simulated Black Shale Distribution

Inclusion of the coupled OMEN-SED model allows us to make prognostic projections of the preservation of OM in accumulating marine sediments in cGENIE, and hence the global distribution of black shales. Essentially, we are now able to forward proxy model key sedimentological features rather than having to make the assumption that black shale occurrence in the geological record can be equated with modeled occurrence of ocean floor anoxia, as was previously the state-of-the-art in paleo Earth system modeling (Monteiro et al., 2012). We find that even without including the influence of OM sulfurization and assuming a highly simplistic globally uniform, and open-ocean Paleogene relevant detrital accumulation rate in marine sediments,

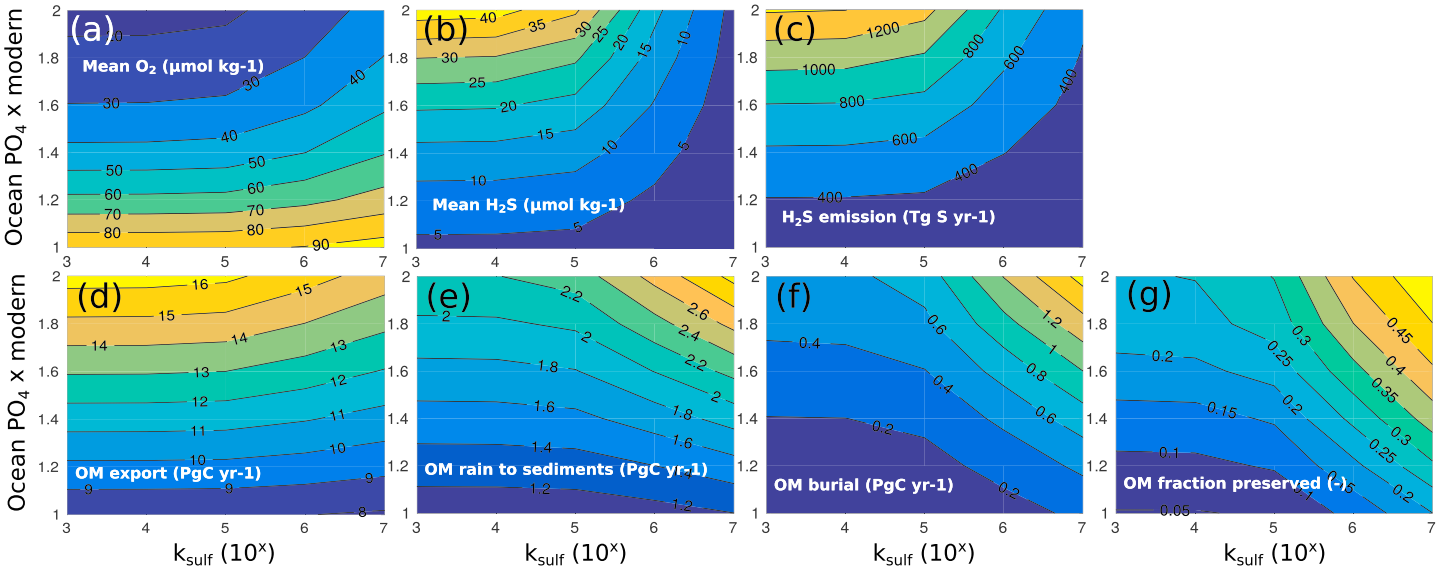

Figure 2. Global values of mean ocean $[O_2]$ (a) and $[H_2S]$ (b), total H_2S emission (c), OM export production (d), OM rain to (e) and its burial in (f) the sediments, and the fraction of OM-preserved/OM-rain (g) as function of sulfurization rate constant and oceanic $[PO_4]$.

our simulated distributions of black shales are in good agreement with compiled observations (Figure 1 and Table 1). Prior to the onset of OAE2, total organic carbon (TOC) contents were already elevated in the proto-North Atlantic Ocean with contents that can reach up to 10 wt% locally (e.g., Kuypers et al., 2002; Sinninghe Damsté & Köster, 1998). Model results show comparable TOC contents in the proto-North Atlantic regions where seafloor anoxia is simulated in the model (Figure 1a and Table 1). Conversely, both observations and model results reveal low TOC contents (generally <1 wt%) for most of the Tethys Sea and especially shallow waters in the north, the proto-South Atlantic, as well as the Indian and Pacific Oceans (Figure 1a). Under peak-OAE conditions, increased TOC contents and laminated black shales occur globally (Figure 1b and Table 1), with particularly high TOC contents reported in the proto-North Atlantic Ocean, the proto-South Atlantic, and the Tethys Sea. Simulated TOC contents reach >20 wt% in parts of the proto-Atlantic Ocean and the Tethys Sea, as well as most of the equatorial regions of the Pacific Ocean, qualitatively paralleling these observations. Conversely, no black shale deposition is simulated in the shallower northern Tethys Sea. The degree of general agreement between observations and model results has two reasons. First, the ocean model presumably projects plausible patterns of Cretaceous seafloor oxygenation state, an inference supported by previous work contrasting cGENIE simulations with the I/Ca oxygenation proxy (Zhou et al., 2015). This, in turn, leads to the absence of OM preservation in oxic conditions due to the higher OM degradation rate constant used in OMEN-SED. Second, for anoxic seafloor conditions the OM degradation rate constant in OMEN-SED has been tuned in order to match observed TOC contents with simulated values. Hence, while the magnitude of projected TOC wt% has been deliberately tuned, the spatial pattern largely arises from the distribution of environmental conditions projected by cGENIE for the Cretaceous.

3.2. The Role of Organic Matter Sulfurization

When we enable OM sulfurization, we find that reaction rates at the lower end of our considered range (i.e., $k_{sulf} \leq 10^4$ M^{-1} $year^{-1}$) do not exert a significant influence on the redox state of the global ocean and OM burial. However, faster OM sulfurization rates (i.e., $k_{sulf} \geq 10^5$ M^{-1} $year^{-1}$) reduce the availability of labile OM for degradation in the water column (because of its conversion to sulfurized, refractory OM), thus lowering oxidant demand, oxygen consumption, and H_2S production (Figures 2a and 2b). The development of ocean euxinia is further suppressed as H_2S is scavenged from the water column as a consequence of OM sulfurization (Figures 3f–3o). Overall, most OM sulfurization takes place in the upper 1,000 m of the water column (not shown) due to the generally high availability of H_2S and labile OM for sulfurization at these depths.

Increasing the global PO_4 inventory and thus export production, generally enhances ocean anoxic/euxinic conditions as well as OM rain to and burial in the sediment (Figure 2). However, global export production decreases with increasing values of k_{sulf} (Figure 2d) because less OM is degraded in the upper ocean, deepen-

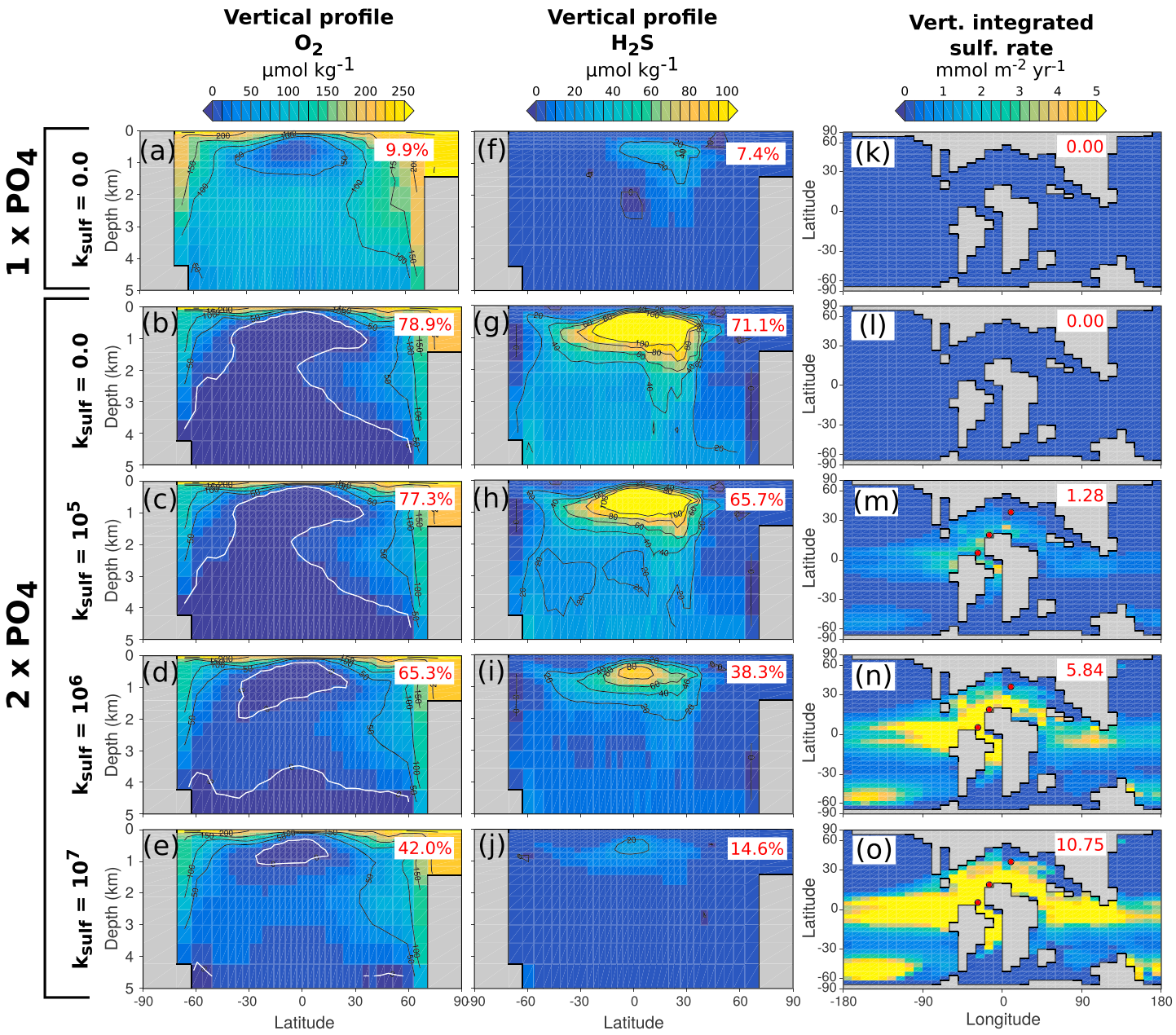

Figure 3. Model sensitivity to k_{sulf}, showing oceanic redox conditions (zonally averaged oxygen (a–e) and hydrogen sulfide (f–j) profiles) and vertically integrated sulfurization rates ((k–o) with global rate of OM sulfurization in mol/year, red dots represent three sections with observed OM sulfurization). White contour in (a)–(e) indicates simulated oxygen concentration of 5 μmol/kg, delimiting the region of ocean anoxia. Percentages indicate fraction of global anoxic ocean volume (a–e) and fraction of global ocean with $[H_2S] > 10$ μmol/kg (f–j).

ing nutrient regeneration and making the return of recycled PO_4 to the surface ocean less efficient. However, total OM rain to, and preservation within, the sediments always increases with k_{sulf} as the bulk OM pool becomes more refractory (Figures 2e–2g). We find that the effect of increasing $[PO_4]$ is to make the system more sensitive to k_{sulf}. The reasons for this increased sensitivity are threefold. First, when PO_4 availability is high, more labile OM is produced and thus available for sulfurization. Second, higher [H2S] in the water column promotes higher sulfurization rates and, third, a nutrient rich ocean can sustain export production even under enhanced OM sulfurization that limits PO_4 recycling. For simulated peak-OAE2 conditions (2 $\times$ PO_4), a moderate OM sulfurization rate of $k_{sulf} = 10^5$ M^{-1} $year^{-1}$ increases OM burial by ~0.16 PgC $year^{-1}$ compared to no sulfurization (k_{sulf} = 10^7 M^{-1} $year^{-1}$ increases burial by ~1.14 PgC $year^{-1}$). These values translate to a 30% increase or more than a tripling of OM burial (Figure 2f). Under these assumptions, the

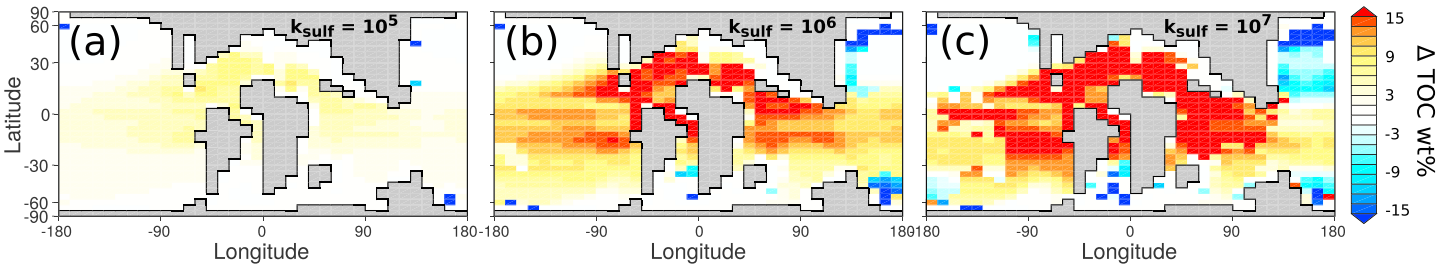

Figure 4. Peak-Ocean Anoxic Event 2 anomaly plots with Figure 1b using different sulfurization rate constants ((a) $k_{sulf} = 10^5$, (b) $k_{sulf} = 10^6$, (c) $k_{sulf} = 10^7$). TOC = total organic carbon.

sedimentary OM preservation efficiency reaches ~30% for $k_{sulf} = 10^5$ M^{-1} $year^{-1}$ and ~55% for $k_{sulf} = 10^7$ M^{-1} $year^{-1}$ (Figure 2g).

We also find that enhanced OM preservation due to rapid OM sulfurization could lead to a significant reoxygenation of the ocean and a ca. 50% decrease in anoxic volume ($[O_2] < 5$ μmol/kg, Figures 3b–3e). The associated reduction in water column euxinia is even more drastic, with the global euxinic volume ($[H_2S] > 10$ μmol/kg) dropping by about 80% (Figures 3g–3j). Our results show substantial spatial variability in water column integrated OM sulfurization rates, a consequence of the spatial distribution of H_2S and labile OM in the model. For instance, highest water column integrated sulfurization rates are simulated in the proto-Atlantic Ocean (Figures 3m–3o) enhancing TOC contents by locally more than 15 TOC wt% compared to the no-sulfurization experiment (Figure 4). Observations generally confirm the occurrence of black shales with high TOC contents in these provinces (Figure 1b and Table 1) and the three sections with observed OM sulfurization are located in areas with elevated sulfurization rates (Figures 3m–3o). Conversely, lowest water column integrated sulfurization rates occur in the high latitudes of the Pacific and Southern Ocean, a consequence of deep-water formation and thus the absence of euxinic conditions in these areas (Monteiro et al., 2012).

4. Discussion

4.1. Significance of Fast Sulfurization for OM Burial During OAE2

Our Earth system model-based investigation supports the hypothesis that rapid OM sulfurization (i.e., $k_{sulf} \geq 10^5$ M^{-1} $year^{-1}$) is important to the formation of Cretaceous black shales in productive and/or semirestricted, euxinic environments (Arndt et al., 2009; Kolonic et al., 2002; Raven et al., 2018). Assuming a plausible range of oceanic H_2S concentrations between 10 and 100 μM, a threshold sulfurization rate constant of 10^5 M^{-1} $year^{-1}$ for the onset of globally important impacts translates to a first-order rate constant of 1.0–10.0 $year^{-1}$. This is two to five orders of magnitude higher than empirically determined rate constants for slow, diagenetic OM sulfurization ($2{\cdot}10^{-4}$ $year^{-1}$, Werne et al., 2000; $1.3{\cdot}10^{-2}$ $year^{-1}$, Sinninghe Damsté et al., 2007). However, our rate constant is in good agreement with more recent studies in the Cariaco Basin, which show that reduced sulfur can be rapidly incorporated into OM in the water column within days or less (Li et al., 2011; Raven et al., 2016).

The impact of rapid OM sulfurization is to drive up to a threefold increase in global carbon burial rates, making this process potentially key to OAE recovery. We find that even relatively subtle changes in $[PO_4]$ and hence export production, in combination with rapid OM sulfurization, have the potential to cause substantial changes in global OM burial (e.g., a 20% increase in $[PO_4]$ from ×1 to ×1.2 driving an approximate doubling of OM burial at the highest rates of k_{sulf}, Figure 2f). Furthermore, increased OM burial due to OM sulfurization is not globally uniform but has a strong local response (Figure 4). Simulated OM preservation efficiencies are specifically enhanced in euxinic areas of the ocean (depending on k_{sulf} ranging from 70% to 100%, Figure 5) and compare well with predicted preservation efficiencies for OAE2 black shales from Demerara Rise (79% to 89%, Arndt et al., 2006, 2009).

Considering the implications of our results to the event as a whole—assuming even just a moderate sulfurization rate constant ($k_{sulf} = 10^5$ M^{-1} $year^{-1}$)—we predict excess peak-OAE2 (×2 PO_4) OM burial of 0.630 PgC $year^{-1}$ above the pre-OAE2 background (×1 PO_4) OM burial rate of 0.061 PgC $year^{-1}$. This translates to 5.25×10^{13} mol C $year^{-1}$ and is thus one order of magnitude higher than the excess burial rate of 0.32×10^{13} mol C $year^{-1}$ calculated by Arthur et al. (1988). However, it needs to be considered that our results are

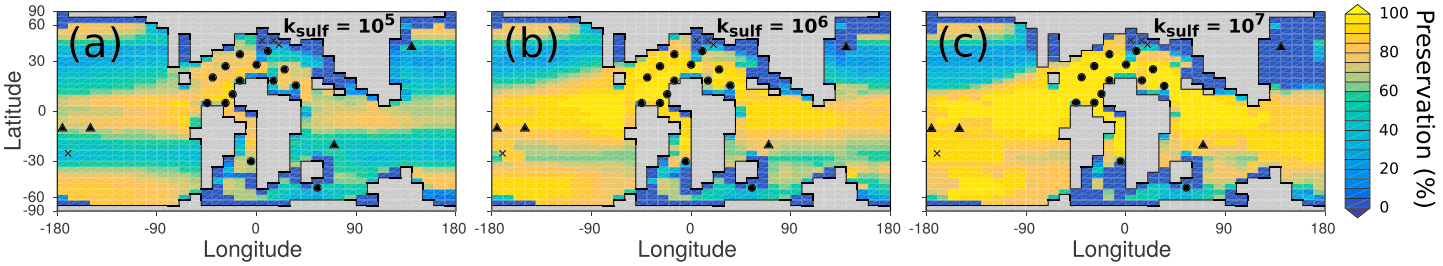

Figure 5. Preservation efficiency of organic matter calculated as the fraction between mean OM concentration in the first 5 cm and OM concentration at 1 m in the sediments using different sulfurization rate constant ((a) $k_{sulf} = 10^5$, (b) $k_{sulf} = 10^6$, (c) $k_{sulf} = 10^7$).

more likely representative for the maximum extent of ocean anoxia/euxinia, thus simulating maximum OM burial rates during the peak-OAE2 event. These maximum rates would not be sustained for the complete recovery phase from peak-OAE2 and then instantaneously drop to background rates. It is more likely that repetitive changes in the redox stratification, due to changes in primary productivity and/or ocean circulation, fostered periodically enhanced OM sulfurization and preservation in a highly dynamic ocean system. We expect that areas already characterized by low O_2 quickly tip over and become carbon burial hotspots. Overall burial rates would gradually decrease from these maximum rates during ocean reoxygenation.

4.2. Transient Effects of OM Sulfurization

While our steady-state ensemble analysis allows us, for the first time, to quantify the magnitude and spatial patterns of OM sulfurization, it tells us little regarding how impacts might evolve on geological time scales (e.g., >10,000 years), nor about how important feedbacks induced by the introduction of this new mechanism are to marine carbon cycling. To address this, we present additional model analysis exploring the transient impacts of OM sulfurization. Sulfurization of organic matter effects ocean biogeochemistry and climate in three main ways: First, it has a direct impact via the enhanced burial of organic carbon (C_{org}) and hence atmospheric CO_2 drawdown and climate cooling. This should act as a negative feedback on sulfurization, as cooling will tend to drive higher oxygen solubility and hence a reduced euxinic area. Second, there is an indirect impact via the ocean alkalinity inventory, caused by the permanent burial of H_2S. The burial of sulfurized OM prevents the reoxidation of the scavenged H_2S, which would reverse the gain of alkalinity caused by sulfate reduction (SO_4^{2-} reduced to H_2S). If sulfate reduction is never reversed because the H_2S is removed through sulfurization and burial, this represents a permanent alkalinity gain by the ocean. In turn, increasing ocean alkalinity drives a shift in carbonate chemistry, away from dissolved carbon dioxide ($CO_{2(aq)}$) and toward carbonate ions (CO_3^{2-}), lowering atmospheric pCO_2 (e.g., Zeebe & Wolf-Gladrow, 2001). This also represents a negative feedback on sulfurization, again via cooling and higher oxygen solubility. Finally, burial of organic phosphorus (P_{org}) contained in sulfurized OM may decrease the oceanic nutrient content and thus organic matter export production. However, the result of this is more complex, because while lower organic matter export will tend to reduce the euxinic ocean volume, it will also drive higher atmospheric pCO_2 and hence warming—a positive feedback on euxinia and OM sulfurization. One of the important roles of mechanistic models in paleoceanography is clearly then to help elucidate the net impact and dynamics of multiple interacting feedbacks in the Earth system (e.g., see for an analogy Jickells et al., 2005; Ridgwell, 2003).

To explore these feedbacks, both in isolation and combination, we perform a series of "open"-system simulations, that is, where atmospheric CO_2 is not prescribed but can evolve in response to an imbalance between inputs (kerogen weathering) and outputs (OM burial). Atmospheric xO_2 is still restored to modern concentrations (21,000 ppm). Given the large reservoir of oxygen in the atmosphere (ca. 3.7×10^{19} mol O_2) as compared to the maximum burial rate of organic carbon in our model ($<1.4 \times 10^{14}$ mol C year^{-1}, Figure 2f), we do not expect this assumption to have any great impact on time scales of a few tens of thousands of years. We show the results of simulations run for 30,000 years and started from the closed-system peak-OAE2 simulation (×2 PO_4) without OM sulfurization (the "spin-up," compare, e.g., Figures 3b, 3g, and 3l). We prescribe a constant global kerogen weathering flux of 0.534 PgC year^{-1} in the open simulations which represents the diagnosed OM burial rate at the end of the spin-up. Any carbon burial simulated beyond this is a net sink of carbon from the system.

Table 2
Sulfurization Related Feedbacks Represented in the Four Transient Sulfurization Experiments (#1–#4) and the Control Experiment (#5)

Experiment	C_{org} burial	P_{org} burial	H_2S burial	permanent ALK gain
#1	✓	–	✓	✓
#2	✓	✓	✓	✓
#3	✓	–	✓	–
#4	✓	✓	✓	–
#5	–	–	–	–

We run a total of four different sulfurization experiments (summarized in Table 2), for which we pick a moderate sulfurization rate constant of $k_{sulf} = 10^5\ M^{-1}\ year^{-1}$ for each. Each sulfurization experiment includes a different combination of feedbacks (Table 2). The first sulfurization experiment (#1) includes excess C_{org} removal associated with the burial of sulfurized OM, but with all P_{org} raining down on the seafloor still instantaneously recycled back to the overlying ocean. The second sulfurization experiment (#2) is the same, but now also accounts for P-loss by assuming that all P_{org} in sulfurized OM is permanently buried in the sediments. The third and fourth experiments are the same as the first two, except now we eliminate the permanent ocean alkalinity gain associated with buried sulfurized OM in order to focus on the more direct effect of sulfurization on OM burial alone. We implement these additional two experiments (#3 and #4) by prescribing a negative flux of alkalinity from the sediments back to the ocean that is set equal to twice the loss of sulfur associated with sulfurized OM burial. In other words, we correct ocean alkalinity for the buried H_2S, that would otherwise have been reoxidized in the water column back to SO_4^{2-} and thereby removing (two moles of) alkalinity, but instead is scavenged and permanently lost form the system. In addition, we run a fifth experiment (#5) in which OM sulfurization does not occur and thus serves as a control.

For the sulfurization experiment #3 which only accounts for C_{org} burial (red dashed line), we find that the initial response compared to the control experiment is, as expected, an increase in OM burial (Figure 6d). The enhanced loss of carbon drives a decline in atmospheric pCO_2 (Figure 6c) and thereby causing global mean temperatures to decrease (Figure 6a + 6b). Cooler temperatures, together with reduced OM degradation rates resulting from a transfer of organic matter from the labile to the sulfurized pool as it settles through the water column, act to increase oceanic O_2 (Figure 6e) and induce further H_2S decrease in addition to the scavenging associated with OM sulfurization (Figure 6g). The observed decrease in alkalinity (Figure 6i) reflects the decrease in oceanic H_2S. However, overall, the decrease in oceanic SO_4^{2-} reflects the dominance of permanent burial of S within sulfurized OM (Figure 6f). Higher global rates of OM burial as compared to rates of kerogen weathering explain the observed decrease in oceanic DIC (Figure 6j). As expected, OM burial rates gradually decrease during ocean reoxygenation (Figure 6d + 6e).

In sulfurization experiment #4 which includes both C_{org} and P_{org} burial (green dashed line), oceanic PO_4 declines over time (to $1.36 \times [PO_4]$ after 30 ka, Figure 6h) and thus causes a decline in export production. Due to the decreased oxidant demand in the water column, reoxygenation of the ocean occurs faster than in the C_{org}-only experiment #3 (Figure 6e + 6g). In combination, this leads to OM burial rates decreasing faster from the maximum rate, eventually dropping below the control experiment (Figure 6d) and thus the constant kerogen weathering flux. Therefore, when considering P_{org} burial, atmospheric pCO_2 (and eventually oceanic DIC) increases above the control-experiment concentration, corresponding to increases in mean temperatures (Figure 6a + 6b).

When we now allow the ocean to permanently gain alkalinity (experiments #1 and #2), we see a dramatic and progressive rise in the oceanic alkalinity inventory (dotted lines in Figure 6i). This is a consequence of SO_4^{2-} being progressively reduced to H_2S in combination with a proportion of this H_2S reacting with labile OM and being permanently buried. As a result of the alkalinity increase, the ocean experiences a higher capacity to sequester and store CO_2, leading to a very rapid decline in atmospheric pCO_2 (Figure 6c) and mean temperatures (Figure 6a + 6b) which drives a more efficient ocean reoxygenation (Figure 6e + 6g). For a constant oceanic PO_4 inventory (experiment #1) this trend is sustained for the entire simulation (red dotted line). When also allowing for P_{org} burial (experiment #2, green dotted line), as PO_4 is lost from the ocean, the decline in export production eventually dominates over the alkalinity gain, causing an increase in atmospheric pCO_2 and temperatures together with ocean reoxygenation.

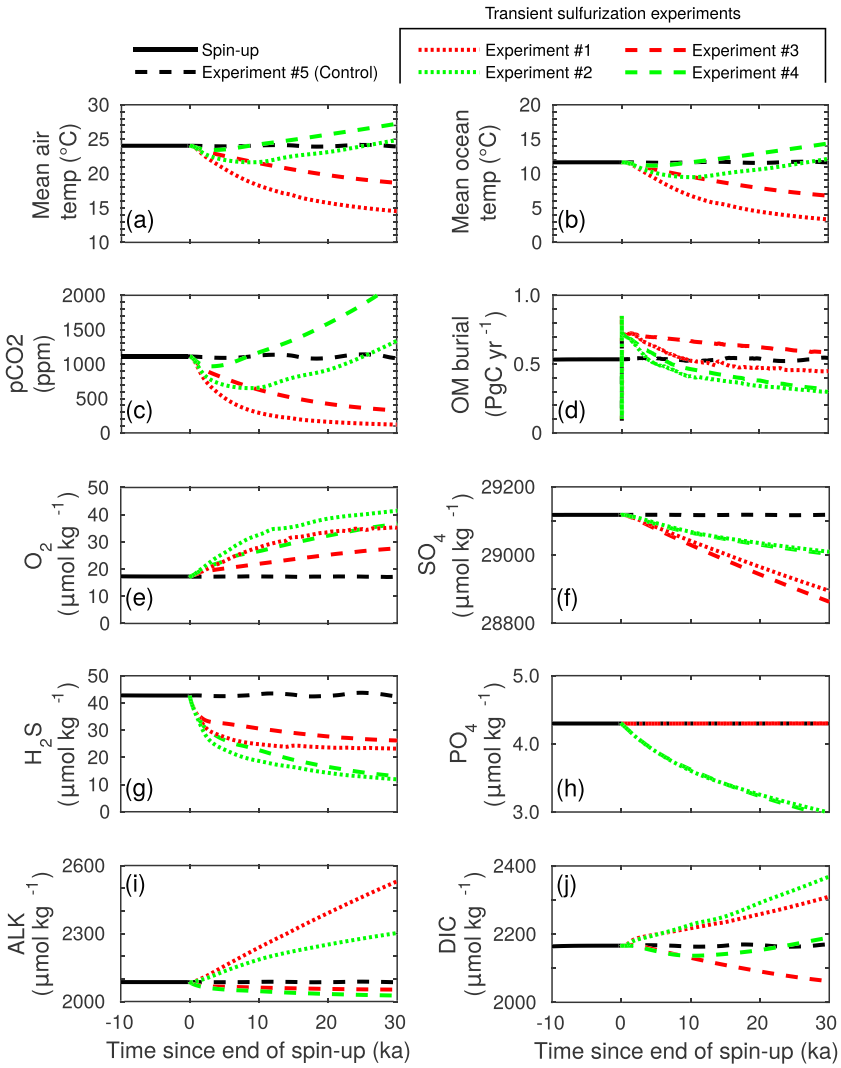

Figure 6. Evolution of atmospheric and oceanic conditions for the last 10 ka of the spin-up (solid black line) and the 30 ka transient control and sulfurization experiments ((a) mean air temperature, (b) mean ocean temperature, (c) atmospheric pCO^2, (d) organic matter burial, (e) mean ocean O^2, (f) mean ocean SO^4, (g) mean ocean H^2S, (h) mean ocean PO^4, (i) mean ocean alkalinity, (j) mean ocean dissolved inorganic carbon). For the feedbacks represented in the transient simulations see Table 2.

Our experiments highlight an unexpected result—that is, as H_2S is permanently lost from the system and prevented from reoxidizing back to sulfate, alkalinity is progressively gained by the ocean. This drives a profound decrease in atmospheric pCO_2 on a time scale of just a few tens of thousands of years. While this effect can be ameliorated if matched by progressive loss of nutrients and declining productivity in the ocean, it should be noted that we have not considered the phosphate regeneration feedback under anoxic conditions here (Van Cappellen & Ingall, 1994), which would tend to reduce the P-loss and hence weaken the amelioration of alkalinity loss. Furthermore, while open in terms of carbon, alkalinity, and nutrients, these experiments lack an sedimentary cycle of calcium carbonate ($CaCO_3$). We are hence missing an additional negative feedback on alkalinity—carbonate compensation (Ridgwell & Zeebe, 2005)—in which as alkalinity and carbonate saturation increase, the preservation and burial of $CaCO_3$ in marine sediments would increase, removing alkalinity at twice the rate of carbon (as $CaCO_3$) and creating a tendency for atmospheric pCO_2 to increase.

5. Limitations and Outlook

Although mechanistically based and quantitative, our analysis should be considered only as a first step toward evaluating the potential role and impact of OM sulfurization associated with events such as OAE2. In our closed-system experiments we have taken a deliberately simplified and steady-state numerical model-based approach to simplify and focus the analysis and highlight the key underlying processes. In our open-system experiments we have focused on the intermediate-term (few tens of kyr) implications of sulfurized OM burial for CO_2 sequestration, climate cooling, ocean reoxygenation, and the nutrient and alkalinity inventory of the ocean. There are several important additional feedbacks that ultimately should be considered in the context of the long-term (100–1,000 kyr) dynamical evolution of the system, particularly (1) climate-responsive terrestrial weathering of P-bearing rocks, (2) $CaCO_3$ weathering and burial, and (3) an anoxia related PO_4 regeneration at the ocean-sediment interface. Furthermore, we have omitted consideration of N cycle dynamics that will serve to further modulate the impact of OM sulfurization. We are also missing the ultimate geological feedback on atmospheric pCO_2 and climate-silicate weathering, which would tend to damp the longer-term trends in pCO_2 and surface temperature although on a time scale longer than the pronounced changes we see occurring in our transient simulations (e.g., Lord et al., 2016). Again, Earth system models are needed to untangle the net results and dynamics of all the interacting feedbacks. Future work is planned considering these subcomponents, in isolation and ultimately all combined, in the context of OAE recovery dynamics.

The wider implications of our novel finding of increased ocean oxygenation and substantially reduced water column euxinia due to OM sulfurization warrants further discussion. Kump et al. (2005) showed that large H_2S emissions from an euxinic ocean (>2,000 Tg S $year^{-1}$) triggers a threshold effect causing H_2S to build up rapidly in the atmosphere, leading to an increase in the atmospheric methane lifetime and thus a destruction of the ozone shield. Indeed, in a previous modeling analysis of potential late Permian conditions using an earlier version of the cGENIE Earth system model, Meyer et al. (2008) projected the occurrence of both widespread ocean euxinia and sulfur (as H_2S) fluxes to the atmosphere far exceeding those from volcanism. The importance of this work is helping provide a "common" (land and ocean) kill mechanism for the end-Permian. However, we find that accounting for OM sulfurization in our Late Cretaceous configuration, not only has the potential to reduce ocean euxinia by ~80% (by volume), but also reduce (by threefold to fourfold) H_2S emissions to the atmosphere (Figure 2c). This is not to say that we can rule out an H_2S kill mechanism for the end-Permian, but rather highlight that OM sulfurization, in removing a highly reactive sink for O_2 in the ocean (H_2S), has more direct implications for upper ocean and atmosphere environmental conditions in addition to the secondary impacts via carbon burial and greenhouse gas warming that have previously been the main focus of interest in this mechanism. Better estimates of the impacts of OM sulfurization specifically for the end-Permian H_2S kill mechanism would require using an end-Permian configuration of the model.

6. Conclusions

Our Earth system model simulations show that organic matter sulfurization in the water column can significantly enhance organic carbon burial during OAE2. The analysis demonstrates that rapid sulfurization has the potential to reduce ocean anoxia and euxina, draw down atmospheric CO_2, and cool down the Cretaceous climate. We thus quantify for the first time by means of 3-D Earth system modeling the role of organic matter sulfurization and enhanced organic carbon burial as an emergency escape mechanism from extreme OAE conditions. Due to the simulated reduction of toxic H_2S emissions to the atmosphere we propose that OM sulfurization could also have wider implications, for instance for the end-Permian H_2S kill mechanism. We also highlight an additional mechanism and set of feedbacks induced by permanent H_2S removal from the ocean—an increase in ocean alkalinity and with it lower pCO_2 and a cooler climate. Overall, the myriad of potential feedbacks that operate in a marine system comprising cycles only of carbon, alkalinity, oxygen, phosphate, and sulfur offer a clear answer to why numerical and particularly Earth system models have considerable utility in paleo studies.

Acknowledgments
We would like to thank two anonymous reviewers for very constructive comments which has led to a significantly improved and more interesting paper. D. H. and A. R. were supported by a Heising-Simons Foundation award. S. A. acknowledges funding from NERC (NE/I021322/1) and the European Union Horizon 2020 research and innovation programme under the Marie Skłodowska-Curie grant agreement 643052. A. R. also acknowledges support from EU grant ERC-2013-CoG-617313. The code for the cGENIE.muffin model is hosted on GitHub. The specific version used in this paper is assigned a DOI (https://doi.org/10.5281/zenodo.2575070). A corresponding user manual detailing installation, configuration, and tutorials is available from GitHub website (https://github.com/derpycode/muffindoc). The data used in this paper are available in the supporting information.

References

Adam, P., Philippe, E., & Albrecht, P. (1998). Photochemical sulfurization of sedimentary organic matter: A widespread process occurring at early diagenesis in natural environments? *Geochimica et Cosmochimica Acta*, *62*(2), 265–271.

Arndt, S., Brumsack, H.-J., & Wirtz, K. W. (2006). Cretaceous black shales as active bioreactors: A biogeochemical model for the deep biosphere encountered during ODP Leg 207 (Demerara Rise). *Geochimica et Cosmochimica Acta*, *70*(2), 408–425.

Arndt, S., Hetzel, A., & Brumsack, H.-J. (2009). Evolution of organic matter degradation in Cretaceous black shales inferred from authigenic barite: A reaction-transport model. *Geochimica et Cosmochimica Acta*, *73*(7), 2000–2022.

Arthur, M. A., Dean, W. E., & Pratt, L. M. (1988). Geochemical and climatic effects of increased marine organic carbon burial at the Cenomanian/Turonian boundary. *Nature*, *335*(6192), 714–717.

Berner, R. A. (1999). A new look at the long-term carbon cycle. *GSA Today*, *9*(11), 1–6.

Böttcher, M. E., Hetzel, A., Brumsack, H.-J., & Schipper, A. (2006). Sulfur-iron carbon geochemistry in sediments of the Demerara Rise. Odp scientific results (Vol. 207, pp. 1 2).

Bowen, G. J., & Zachos, J. C. (2010). Rapid carbon sequestration at the termination of the Palaeocene-Eocene Thermal Maximum. *Nature Geoscience*, *3*(12), 866–869.

Brumsack, H.-J. (2006). The trace metal content of recent organic carbon-rich sediments: Implications for Cretaceous black shale formation. *Palaeogeography, Palaeoclimatology, Palaeoecology*, *232*, 344–361. https://doi.org/10.1016/j.palaeo.2005.05.011

Demaison, G. J., & Moore, G. T. (1980). Anoxic environments and oil source bed genesis. *Organic Geochemistry*, *2*(1), 9–31.

Edwards, N. R., & Marsh, R. (2005). Uncertainties due to transport-parameter sensitivity in an efficient 3-D ocean-climate model. *Climate Dynamics*, *24*(4), 415–433. https://doi.org/10.1007/s00382-004-0508-8

Flögel, S., Wallmann, K., Poulsen, C. J., Zhou, J., Oschlies, A., Voigt, S., & Kuhnt, W. (2011). Simulating the biogeochemical effects of volcanic CO2 degassing on the oxygen-state of the deep ocean during the Cenomanian/Turonian Anoxic Event (OAE2). *Earth and Planetary Science Letters*, *305*(3-4), 371–384.

Friedrich, O., Norris, R. D., & Erbacher, J. (2012). Evolution of middle to Late Cretaceous oceans A 55 m.y. record of Earth's temperature and carbon cycle. *Geology*, *40*(2), 107–110.

Goldberg, T., Poulton, S. W., Wagner, T., Kolonic, S. F., & Rehkämper, M. (2016). Molybdenum drawdown during Cretaceous Oceanic Anoxic Event 2. *Earth and Planetary Science Letters*, *440*, 81–91.

Gutjahr, M., Ridgwell, A., Sexton, P. F., Anagnostou, E., Pearson, P. N., Pälike, H., et al. (2017). Very large release of mostly volcanic carbon during the Palaeocene-Eocene Thermal Maximum. *Nature*, *548*(7669), 573–577.

Handoh, I. C., & Lenton, T. M. (2003). Periodic mid-Cretaceous oceanic anoxic events linked by oscillations of the phosphorus and oxygen biogeochemical cycles. *Global Biogeochemical Cycles*, *17*(4), 1092. https://doi.org/10.1029/2003GB002039

Hetzel, A., Böttcher, M. E., Wortmann, U. G., & Brumsack, H.-J. (2009). Paleo-redox conditions during OAE 2 reected in Demerara Rise sediment geochemistry (ODP Leg 207). *Palaeogeography, Palaeoclimatology, Palaeoecology*, *273*(3), 302–328. https://doi.org/10.1016/j.palaeo.2008.11.005

Hülse, D., Arndt, S., Daines, S., Regnier, P., & Ridgwell, A. (2018). OMEN-SED 1.0: A novel, numerically efficient organic matter sediment diagenesis module for coupling to Earth system models. *Geoscientific Model Development*, *11*(7), 2649–2689.

Hülse, D., Arndt, S., Wilson, J. D., Munhoven, G., & Ridgwell, A. (2017). Understanding the causes and consequences of past marine carbon cycling variability through models. *Earth-Science Reviews*, *171*, 349–382.

Jenkyns, H. C. (2010). Geochemistry of oceanic anoxic events. *Geochemistry, Geophysics, Geosystems*, *11*, Q03004. https://doi.org/10.1029/2009GC002788

Jickells, T. D., An, Z. S., Andersen, K. K., Baker, A. R., Bergametti, G., Brooks, N., et al. (2005). Global iron connections between desert dust, ocean biogeochemistry, and climate. *Science*, *308*(5718), 67–71.

Kennedy, M. J., Pevear, D. R., & Hill, R. J. (2002). Mineral surface control of organic carbon in black shale. *Science*, *295*(5555), 657–660.

Kok, M. D., Schouten, S., & Sinninghe Damst, J. S. (2000). Formation of insoluble, nonhydrolyzable, sulfur-rich macromolecules via incorporation of inorganic sulfur species into algal carbohydrates. *Geochimica et Cosmochimica Acta*, *64*(15), 2689–2699.

Kolonic, S., Damsté, J. S. S., Böttcher, M. E., Kuypers, M. M. M., Kuhnt, W., Beckmann, B., & Wagner, G. S. T. (2002). Geochemical characterization of Cenomanian/Turonian black shales from the Tarfaya Basin (SW Morocco): Relationships between paleoenvironmental conditions and early sulfurization of sedimentary organic matter. *Journal of Petroleum Geology*, *25*(3), 325–350.

Kolonic, S., Wagner, T., Forster, A., Sinninghe Damsté, J. S., Walsworth-Bell, B., Erba, E., et al. (2005). Black shale deposition on the northwest African Shelf during the Cenomanian/Turonian oceanic anoxic event: Climate coupling an global organic carbon burial. *Paleoceanography*, *20*, PA1006. https://doi.org/10.1029/2003PA000950

Kump, L. R., Pavlov, A., & Arthur, M. A. (2005). Massive release of hydrogen sulfide to the surface ocean and atmosphere during intervals of oceanic anoxia. *Geology*, *33*(5), 397–400.

Kuypers, M. M. M., Pancost, R. D., Nijenhuis, I. A., & Sinninghe Damsté, J. S. (2002). Enhanced productivity led to increased organic carbon burial in the euxinic North Atlantic basin during the late Cenomanian oceanic anoxic event. *Paleoceanography*, *17*(4), 1051. https://doi.org/10.1029/2000PA000569

Kuypers, M. M. M., Pancost, R. D., & Sinninghe Damsté, J. S. (1999). A large and abrupt fall in atmospheric CO2 concentration during Cretaceous times. *Nature*, *399*(6734), 342–345.

LaRowe, D. E., & Van Cappellen, P. (2011). Degradation of natural organic matter: A thermodynamic analysis. *Geochimica et Cosmochimica Acta*, *75*(8), 2030–2042.

Li, X., Cutter, G. A., Thunell, R. C., Tappa, E., Gilhooly, W. P., Lyons, T. W., et al. (2011). Particulate sulfur species in the water column of the Cariaco Basin. *Geochimica et Cosmochimica Acta*, *75*(1), 148–163.

Lord, N. S., Ridgwell, A., Thorne, M. C., & Lunt, D. J. (2016). An impulse response function for the long tail of excess atmospheric CO2 in an Earth system model. *Global Biogeochemical Cycles*, *30*, 2–17. https://doi.org/10.1002/2014GB005074

Meyer, K. M., & Kump, L. R. (2008). Oceanic euxinia in Earth history: Causes and consequences. *Annual Review of Earth and Planetary Sciences*, *36*(1), 251–288. https://doi.org/10.1146/annurev.earth.36.031207.12%4256

Meyer, K. M., Kump, L. R., & Ridgwell, A. (2008). Biogeochemical controls on photic-zone euxinia during the end-Permian mass extinction. *Geology*, *36*(9), 747–750.

Meyer, K. M., Ridgwell, A., & Payne, J. L. (2016). The inuence of the biological pump on ocean chemistry: Implications for long-term trends in marine redox chemistry, the global carbon cycle, and marine animal ecosystems. *Geobiology*, *14*(3), 207–219. https://doi.org/10.1111/gbi.12176

Monteiro, F. M., Pancost, R. D., Ridgwell, A., & Donnadieu, Y. (2012). Nutrients as the dominant control on the spread of anoxia and euxinia across the Cenomanian-Turonian oceanic anoxic event (OAE2): model-data comparison. *Paleoceanography*, *27*, PA4209. https://doi.org/10.1029/2012PA002351

Moodley, L., Middelburg, J. J., Herman, P. M. J., Soetaert, K., & de Lange, G. J. (2005). Oxygenation and organic-matter preservation in marine sediments: Direct experimental evidence from ancient organic carbon rich deposits. *Geology*, *33*(11), 889–892.

Naafs, B. D. A., Castro, J. M., Gea, G. A. D., Quijano, M. L., Schmidt, D. N., & Pancost, R. D. (2016). Gradual and sustained carbon dioxide release during Aptian Oceanic Anoxic Event 1a. *Nature Geoscience*, *9*(2), 135–139. https://doi.org/10.1038/ngeo2627

Owens, J. D., Lyons, T. W., Li, X., Macleod, K. G., Gordon, G., Kuypers, M. M. M., et al. (2012). Iron isotope and trace metal records of iron cycling in the proto-North Atlantic during the Cenomanian-Turonian oceanic anoxic event (OAE-2). *Paleoceanography*, *27*, PA3223. https://doi.org/10.1029/2012PA002328/abstract

Pancost, R. D., Crawford, N., Magness, S., Turner, A., Jenkyns, H. C., & Maxwell, J. R. (2004). Further evidence for the development of photiczone euxinic conditions during Mesozoic oceanic anoxic events. *Journal of the Geological Society*, *161*(3), 353–364. https://doi.org/10.1144/0016764903-059

Pedersen, T. F., & Calvert, S. E. (1990). Anoxia vs. productivity: What controls the formation of organic-carbon-rich sediments and sedimentary rocks? (1). *AAPG Bulletin*, *74*(4), 454–466.

Pogge von Strandmann, P. A. E., Jenkyns, H. C., & Woodfine, R. G. (2013). Lithium isotope evidence for enhanced weathering during Oceanic Anoxic Event 2. *Nature Geoscience*, *6*(8), 668–672.

Raven, M. R., Fike, D. A., Gomes, M. L., Webb, S. M., Bradley, A. S., & McClelland, H.-L. O. (2018). Organic carbon burial during OAE2 driven by changes in the locus of organic matter sulfurization. *Nature Communications*, *9*(1), 3409.

Raven, M. R., Sessions, A. L., Adkins, J. F., & Thunell, R. C. (2016). Rapid organic matter sulfurization in sinking particles from the Cariaco Basin water column. *Geochimica et Cosmochimica Acta*, *190*, 175–190.

Ridgwell, A. (2003). Implications of the glacial CO2 "iron hypothesis" for Quaternary climate change. *Geochemistry, Geophysics, Geosystems*, *4*(9), 1076. https://doi.org/10.1029/2003GC000563

Ridgwell, A., Hargreaves, J. C., Edwards, N. R., Annan, J. D., Lenton, T. M., Marsh, R., et al. (2007). Marine geochemical data assimilation in an efficient Earth System Model of global biogeochemical cycling. *Biogeosciences*, *4*(1), 87–104.

Ridgwell, A., & Zeebe, R. E. (2005). The role of the global carbonate cycle in the regulation and evolution of the Earth system. *Earth and Planetary Science Letters*, *234*(3-4), 299–315.

Ruvalcaba Baroni, I., Topper, R. P. M., van Helmond, N. A. G. M., Brinkhuis, H., & Slomp, C. P. (2014). Biogeochemistry of the North Atlantic during oceanic anoxic event 2: Role of changes in ocean circulation and phosphorus input. *Biogeosciences*, *11*(4), 977–993.

Schlanger, S., & Jenkyns, H. (1976). Cretaceous oceanic anoxic events: Causes and consequences. *Geologie en Mijnbouw*, *55*(3-4), 179–184.

Sinninghe Damsté, J. S., Irene, W., Rijpstra, C., de Leeuw, J. W., & Schenck, P. A. (1988). Origin of organic sulphur compounds and sulphur-containing high molecular weight substances in sediments and immature crude oils. *Organic Geochemistry*, *13*(4), 593–606.

Sinninghe Damsté, J. S., Kok, M. D., Köster, J., & Schouten, S. (1998). Sulfurized carbohydrates: An important sedimentary sink for organic carbon? *Earth and Planetary Science Letters*, *164*(1–2), 7–13.

Sinninghe Damsté, J. S., & Köster, J. (1998). A euxinic southern North Atlantic Ocean during the Cenomanian/Turonian oceanic anoxic event. *Earth and Planetary Science Letters*, *158*(3–4), 165–173.

Sinninghe Damsté, J. S., Rijpstra, W. I. C., Coolen, M. J. L., Schouten, S., & Volkman, J. K. (2007). Rapid sulfurisation of highly branched isoprenoid (HBI) alkenes in sulfidic Holocene sediments from Ellis Fjord, Antarctica. *Organic Geochemistry*, *38*(1), 128–139.

Tsandev, I., & Slomp, C. P. (2009). Modeling phosphorus cycling and carbon burial during Cretaceous Oceanic Anoxic Events. *Earth and Planetary Science Letters*, *286*(1-2), 71–79.

Van Cappellen, P., & Ingall, E. D. (1994). Benthic phosphorus regeneration, net primary production, and ocean anoxia: A model of the coupled marine biogeochemical cycles of carbon and phosphorus. *Paleoceanography*, *9*(5), 677–692. https://doi.org/10.1029/94PA01455

van Dongen, B. E., Schouten, S., Baas, M., Geenevasen, J. A. J., & Sinninghe Damst, J. S. (2003). An experimental study of the low-temperature sulfurization of carbohydrates. *Organic Geochemistry*, *34*(8), 1129–1144.

van Dongen, B. E., Schouten, S., & Sinninghe Damsté, J. S. (2006). Preservation of carbohydrates through sulfurization in a Jurassic euxinic shelf sea: Examination of the Blackstone Band TOC cycle in the Kimmeridge Clay Formation, UK. *Organic Geochemistry*, *37*(9), 1052–1073.

van Kaam-Peters, H. M. E, Schouten, S., de Leeuw, J. W., & Sinninghe Damsté, J. S. (1997). A molecular and carbon isotope biogeochemical study of biomarkers and kerogen pyrolysates of the Kimmeridge Clay Facies: Palaeoenvironmental implications. *Organic Geochemistry*, *27*(7), 399–422.

van Kaam-Peters, H. M. E, Schouten, S., Köster, J., & Sinninghe Damsté, J. S. (1998). Controls on the molecular and carbon isotopic composition of organic matter deposited in a Kimmeridgian euxinic shelf sea: Evidence for preservation of carbohydrates through sulfurisation. *Geochimica et Cosmochimica Acta*, *62*(19), 3259–3283.

Volk, T., & Hoffert, M. I. (1985). Ocean carbon pumps: Analysis of relative strengths and efficiencies in ocean-driven atmospheric CO_2 changes. In E. T. Sundquist & W. S. Broecker (Eds.), *The carbon cycle and atmospheric CO_2: Natural variations Archean to present, Geophysical Monograph Series* (Vol. 32, pp. 99–110). Washington, DC: American Geophysical Union.

Wakeham, S. G., Sinninghe Damsté, J. S., Kohnen, M. E. L., & De Leeuw, J. W. (1995). Organic sulfur compounds formed during early diagenesis in Black Sea sediments. *Geochimica et Cosmochimica Acta*, *59*(3), 521–533.

Wallmann, K. (2001). Controls on the Cretaceous and Cenozoic evolution of seawater composition, atmospheric CO2 and climate. *Geochimica et Cosmochimica Acta*, *65*(18), 3005–3025.

Werne, J. P., Hollander, D. J., Behrens, A., Schaeffer, P., Albrecht, P., & Sinninghe Damsté, J. S. (2000). Timing of early diagenetic sulfurization of organic matter: A precursor-product relationship in Holocene sediments of the anoxic Cariaco Basin, Venezuela. *Geochimica et Cosmochimica Acta*, *64*(10), 1741–1751.

Zeebe, R. E., & Wolf-Gladrow, D. (2001). *CO2 in seawater: Equilibrium, kinetics, isotopes: Equilibrium, kinetics, isotopes: Elsevier Oceanographic Series* (Vol. 65). New York: Elsevier.

Zeebe, R. E., & Zachos, J. C. (2007). Reversed deep-sea carbonate ion basin gradient during Paleocene-Eocene thermal maximum. *Paleoceanography*, *22*, PA3201. https://doi.org/10.1029/2006PA001395

Zhou, X., Jenkyns, H. C., Owens, J. D., Junium, C. K., Zheng, X.-Y., Sageman, B. B., et al. (2015). Upper ocean oxygenation dynamics from I/Ca ratios during the Cenomanian-Turonian OAE 2. *Paleoceanography*, *30*, 510–526. https://doi.org/10.1002/2014PA002741